Heat and Mass Transfer 38 (2002) 369–377 © Springer-Verlag 2001
DOI 10.1007/s002310100224

Numerical simulation of fully developed turbulent flow and heat transfer in annular-sector ducts

Z.-Y. Li, T.-C. Hung, W.-Q. Tao

Abstract The mixing length theory is employed to simulate the fully developed turbulent heat transfer in annular-sector ducts with five apex angles ($\theta_0 = 18, 20, 24, 30, 40^\circ$) and four radius ratios ($R_o/R_i = 2, 3, 4, 5$). The Reynolds number range is 10^4–10^5. The numerical results agree well with an available correlation which was obtained in following parameter range: $\theta_0 = 18, 20, 24, 30, 40^\circ$, $R_o/R_i = 4$ and $Re = 10^4$–5×10^4. The present work demonstrates that the application range of the correlation can be much extended. Apart from the mixing length theory, the k–ε model with wall function and the Reynolds stress model are also employed. None of the friction factor results predicted by the three models agrees well with the test data. For the heat transfer prediction the mixing length theory seems the best for the cases studied.

1 Introduction

Internally finned tubes are widely used for enhancing heat transfer, particularly in power and chemical engineering, petroleum industry, and air-conditioning systems. Finned annulus is one of such geometry. When the fins span the full radial width of the annulus, the finned construction becomes a multi-passage channel [1, 2], in which every passage is annular-sector in shape (see Fig. 1a). Heat transfer and fluid flow characteristics in ducts with non-circular cross-section have been extensively studied in the past, and comprehensive reviews have been made in [2–4]. In the following only the works related to fluid flow and the heat transfer in the annular-sector ducts are briefly reviewed.

Sparrow et al. provided their analytical solution for fRe of laminar flow in annular-sector ducts [1]. Soliman et al. solved the fluid flow problem for the entrance region [5]. Later Soliman [6] and Ben-Ali et al. [7] investigated the fully developed fluid flow and heat transfer for the three kinds of thermal boundary conditions: uniform wall temperature (T); uniform wall flux axially but uniform wall temperature circumferentially (H1); and uniform wall flux both axially and circumferentially (H2). Lin et al. [8] studied the laminar thermal entrance problem for T and H1 boundary conditions. The works mentioned above are all for laminar flow case using numerical or analytical methods. As far as the turbulent heat transfer and fluid flow in annular-sector ducts are concerned, the related works known to the present authors are that by Carnavos [9], and Tao et al. [10]. In the work of Carnavos some data of the over-all heat transfer coefficient and friction factor for a multi-passage annular channel were obtained. Tao et al. experimentally investigated the thermal developing and fully developed turbulent fluid flow and heat transfer for five annular-sector ducts, with apex angle varying from 18 to 40°. In their experiments, the outer surface was electrically heated, while the inner surface was adiabatic. This boundary condition was supposed to simulate the heat transfer in a gas-cooler where the hot gas goes into the annular space and water cools the gas from the outside surface of the annular space. The inner tube of the annulus was used as a supporter for the radial fins and no fluid goes through its inner space. Gas-coolers based on this kind of multi-passage channel with fins further finned at the outside surface of the inner tube are now applied in many heat exchangers for cooling gas. In the work of Tao et al. a correlation for the fully developed turbulent heat transfer was provided. The correlation was based on their test data in the following parameter range: $Re = 10^4$–5×10^4, Pr = 0.7, $R_o/R_i = 4$ and $\theta_0 = 18, 20, 24, 30$ and 40°. Since thermally fully developed turbulent heat transfer is often encountered in engineering applications, numerical study on this subject is of essential importance. A search of literature, however, did not find any related numerical works for the fully developed heat transfer in the annular-sector ducts.

The purposes of the present study are three-fold. First, different turbulent models are used, from simple mixing length theory to quite sophisticated Reynolds stress model to simulate the fully developed heat transfer for gas in the parameter range of Tao et al.'s study, so that an appropriate turbulent model can be picked out for the problem studied by comparisons between the numerical results and test data. Then this model is adopted to extend the geometrical range by varying the radius ratio from 2 to 5 and

Received on 17 July 2000 / Published online: 29 November 2001

Z.-Y. Li, T.-C. Hung, W.-Q. Tao (✉)
Xi'an Jiaotong University
Shaanxi, 710049, China
E-mail: wqtao@xjtu.edu.cn

T.-C. Hung
Department of Mechanical Engineering
I-show University
Taiwan, China

This work was supported by the National Key Laboratory of Air-Craft Engine of China and the National Key Project of Fundamental R & D of China (Grant No.20000 26303).

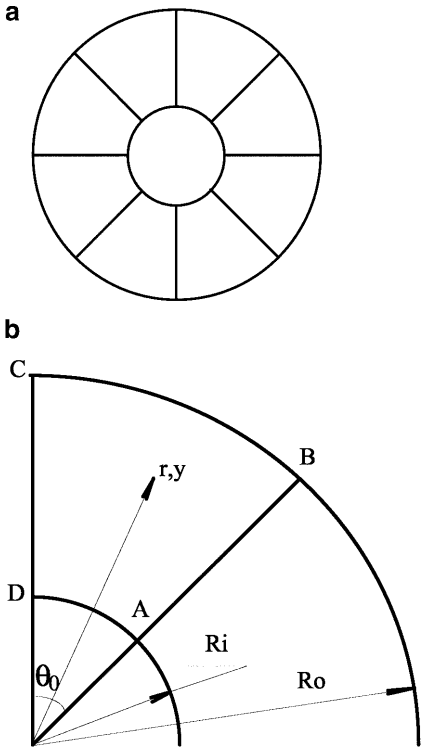

Fig. 1. Geometry of duct investigated. (**a**) Finned annular-sector duct (**b**) Computational domain

Reynolds number from 5×10^4 to 10^5, to further examine whether the correlation provided by Tao et al. can be still used. Finally, the heat transfer and fluid flow characteristics (velocity and temperature contours) are presented based on the numerical results to enhance our understanding on such a basic turbulent heat transfer problem.

2 Mathematical and physical model

For the steady-state, fully developed fluid flow and heat transfer in annular-sector duct (Fig. 1b), ignoring the axial heat conduction, the general governing equations may be written in polar coordinates as [11]:

$$\frac{1}{r}\frac{\partial}{\partial r}\left(r\Gamma_{\text{eff}}\frac{\partial \phi}{\partial r}\right)+\frac{1}{r}\frac{\partial}{\partial \theta}\left(\Gamma_{\text{eff}}\frac{\partial \phi}{r\partial \theta}\right)+S_\phi=0 \qquad (1)$$

where ϕ is the general variable, Γ_{eff} is the effective diffussivity and S_ϕ is the source term. The expressions for Γ_{eff} and S_ϕ are listed in Table 1 [11], in which the standard k–ε model is incorporated.

The turbulent viscosity μ_t is determined by following equation

$$\mu_t = c_\mu \rho k^2/\varepsilon \qquad (2)$$

The constants in Table 1 and Eq. (2) are listed in Table 2.

The mixing length theory

For the flow in the annular-sector duct, velocity gradients exist both in r- and θ-direction. According to the mixing length theory of Prandtl and the method proposed by

Table 1. Expressions for Γ_{eff} and S_ϕ

Transport equations	ϕ	Γ_{eff}	S_ϕ
Continuity equation	1	0	0
Momentum equation	w	$\mu+\mu_t$	$-\mathrm{d}p/\mathrm{d}z$
Energy equation	T	$\mu/\mathrm{Pr}+\mu_T/\sigma_T$	$-\rho w\,\partial T/\partial z$[a]
Turbulent kinetic energy equation	k	$\mu+\mu_t/\sigma_k$	$\mu_t G^2-\rho\varepsilon$
Dissipation rate equation	ε	$\mu+\mu_t/\sigma_\varepsilon$	$\frac{\varepsilon}{k}(c_1 G^2-c_2\rho\varepsilon)$

[a] $\rho w\,\partial T/\partial z=\rho w\vartheta\,\mathrm{d}T_b/\mathrm{d}z$, $\vartheta=\frac{T-T_b}{T_w-T_b}$

[b] $G=(\partial w/\partial r)^2+(\partial w/r\partial\theta)^2$

Table 2. Constants in Table 1 and Eq. (2)

c_μ	σ_k	σ_ε	σ_T	c_1	c_2
0.09	1.00	1.30	0.9	1.44	1.92

Patankar et al. [12], the turbulent viscosity of this case may be determined by following equation:

$$\mu_t=\rho L^2\left[\left(\frac{\partial w}{\partial r}\right)^2+\left(\frac{1}{r}\frac{\partial w}{\partial \theta}\right)^2\right]^{\frac{1}{2}} \qquad (3)$$

where L is the effective mixing length. The determination of L is conducted basically along the line suggested by Patankar et al. [12]. Considering a point with coordinates of (r,θ), see Fig. 1b. First, assuming an annular pipe flow without fins, the mixing length at r is $L_p(r)$, where the subscript p refers to a pipe flow. Next, regarding the two radial surfaces as a wedge-type channel, the mixing length at θ is $L_c(\theta)$, where the subscript c denoting a channel. In the annular-sector duct, the tube wall and radial surface simultaneously influence the mixing length at (r,θ). Thus the effective mixing length must be a kind of superposition of the individual mixing lengths. Since the closer is the point to one of these surfaces, the stronger should be the influence of that surface on the effect mixing length. The superposition of the reciprocals of $L_p(r)$ and $L_c(\theta)$ can meet above-mentioned requirement. Thus we have

$$\frac{1}{L}=\frac{1}{L_p(r)}+\frac{1}{L_c(\theta)} \qquad (4)$$

To consider the damping effect of the molecular viscosity in the vicinity of solid surface, the mixing lengths are each represented as the product of a Nikuradse-type mixing length and the Van Driest damping factor, that is

$$\begin{aligned} L_p(r)&=[1-\exp(y^+/26)]\cdot l_p \\ L_c(\theta)&=[1-\exp(s^+/26)]\cdot l_c \end{aligned} \qquad (5)$$

Attention is now turned to the determination of $l_p(r)$ and $l_c(\theta)$. Considering a fully developed turbulent flow in an annulus with inner radius R_i and outer radius R_o. The velocity is zero at R_i, increases with increasing R, attains a maximum at $R=R_m$, and then decreases to zero at R_o. From this physical intuition, we adopt following mixing

length representation for L_p, which is consisted of two Nikuradse-type expressions for the inner and outer part of the annulus, delineated by the radius R_m: $R_i \le R \le R_m$ and $R_m \le R \le R_o$. Let

$$y = R - R_i, \quad y_m = R_m - R_i, \quad y_{om} = R_o - R_m$$

then l_p can be expressed by

$$l_p = \begin{cases} l_i = [b_1 - b_2(1 - y/y_m)^2 - b_3(1 - y/y_m)^4]y_m, & y \le y_m \\ l_o = [0.14 - 0.08(y - y_m)^2/y_{om}^2 - 0.06(y - y_m)^4/y_{om}^4]y_{om}, & y > y_m \end{cases} \quad (6)$$

where $b_1 = 0.14y_{om}/y_m$, $b_2 = 2b_1 - 0.5\kappa_i$, $b_3 = 0.5\kappa_i - b_1$. The constants in l_o are obviously copied from Nikuradse equation for the mixing length in a tube. The constants in l_i, b_1, b_2, and b_3 are derived from the following physical conditions: (1) $l_i = 0$ at $y = 0$; (2) $\partial l_i/\partial y = \kappa_i$ at $y = 0$; and (3) $l_o = l_i$ at $y = y_m$. The expressions of R_m and κ_i for concentric annular flow are as follows [12]:

$$\frac{\kappa_i}{\kappa} = \frac{(R_o/R_i)}{\Omega - 1}\left[\frac{(R_o/R_i)^2 - \Omega^2}{(R_o/R_i)(\Omega^2 - 1)}\right]^{\frac{1}{2}} \quad (7)$$

$$\Omega = \frac{R_m}{R_o} = \frac{1 + (R_o/R_i)^{0.657}}{1 + (R_o/R_i)^{0.343}} \quad (8)$$

where κ is the von Karman constant (0.4).

It should be noted that Eqs. (7) and (8) are obtained for the concentric annular flow. The value of Ω in this study is iteratively determined during the numerical solution procedure as follows. Numerical simulation is conducted first by using the value from Eq. (8) as an initial one. From the converged solution the position of R_m is searched. If the computed value is appreciably deviated from the predicted one, then computation is repeated until the difference between predicted and computed values of R_m is less than some pre-specified value. In this study a relative difference of 5×10^{-4} was adopted as the allowed difference.

Similarly the mixing length $L_c(\theta)$ can be evaluated by following equation

$$l_c = \begin{cases} [a_1 - a_2(1 - s/s_0)^2 - a_3(1 - s/s_0)^4]s_0, & s \le s_0 = R\theta_0/2 \\ [a_1 - a_2(1 - (s_T - s)s_0)^2 - a_3(1 - (s_T - s)s_0)^4]s_0, & s > s_0, s_T = R\theta_0 \end{cases} \quad (9)$$

where $a_2 = 2a_1 - 0.5\kappa, a_3 = 0.5\kappa - a_1$. In Eq. (9) a_1 is an adjustable constant such that the predicted heat transfer results can meet the test data more closely.

The k–ε model with wall function

In the prediction of the turbulent flow and heat transfer, the k–ε two-equation model in conjunction with the wall function method has been widely used in the literature. This method is also adopted as one of the turbulence models in this study. From many successful computed examples, we found that the problem studied by Yueh and Chieng [13] is quite similar to our case. They predicted the heat transfer characteristics of the flow for CANDU-type 19-rod fuel bundles using this model. In their computation, the dimensionless velocity and distance are defined as follows:

$$w^+ = w_p/\sqrt{\tau_w/\rho} = \frac{1}{\kappa}\ln(Ey_p^+), \quad y_p^+ = \rho y_p\sqrt{\tau_w/\rho/\mu} \quad (10)$$

The turbulent dissipation at the first internal point is determined by

$$\varepsilon_p = c_\mu^{3/4}k_p^{3/2}/\kappa y_p \quad (11)$$

The dimensionless temperature is computed by

$$T^+ = \sigma_T(w^+ + P_{fun}) \ ,$$

$$P_{fun} = 9.0\left[\left(\frac{Pr}{\sigma_T}\right) - 1\right]\left(\frac{Pr}{\sigma_T}\right)^{-0.25} \quad (12)$$

where τ_w is the wall shear stress. It is worth pointing out that in many references adopting wall function method, the definitions of dimensionless velocity and distance usually include the turbulent kinetic energy (see for example, Refs. [11, 14]) and are cited as follows:

$$w^+ = \frac{w_p\left(c_\mu^{0.25}k_p^{0.5}\right)}{\tau_w/\rho} = \frac{1}{\kappa}\ln(Ey_p^+) \ ,$$

$$y_p^+ = \frac{\rho y_p\left(c_\mu^{0.25}k_p^{0.5}\right)}{\mu} \quad (13)$$

However, our preliminary computations showed that using Eq. (10) could lead to numerical results which have a better agreement with the test data. The compared results are shown in Fig. 2.

The Reynolds stress model

We adopted the FLUENT software (version 4.4.8) to predict the fluid flow and heat transfer by the Reynolds stress model. For the steady flow without rotation, the Reynolds stress equations can be written as

$$\begin{aligned} u_k\frac{\partial}{\partial x_k}\left(\overline{u_i'u_j'}\right) &= -\frac{\partial}{\partial x_k}\left[\left(\overline{u_i'u_j'u_k'}\right) + \overline{\frac{p}{\rho}\left(\delta_{kj}u_i' + \delta_{ik}u_j'\right)} - \upsilon\frac{\partial}{\partial x_k}\left(\overline{u_i'u_j'}\right)\right] \\ &\quad - \left[\overline{u_i'u_k'}\frac{\partial u_j}{\partial x_k} + \overline{u_j'u_k'}\frac{\partial u_i}{\partial x_k}\right] + \overline{\frac{p}{\rho}\left(\frac{\partial u_j'}{\partial x_i} + \frac{\partial u_i'}{\partial x_j}\right)} \\ &\quad - 2\upsilon\left(\overline{\frac{\partial u_i'}{\partial x_k}\frac{\partial u_j'}{\partial x_k}}\right) + S_{ij} + D_{ij} \end{aligned} \quad (14)$$

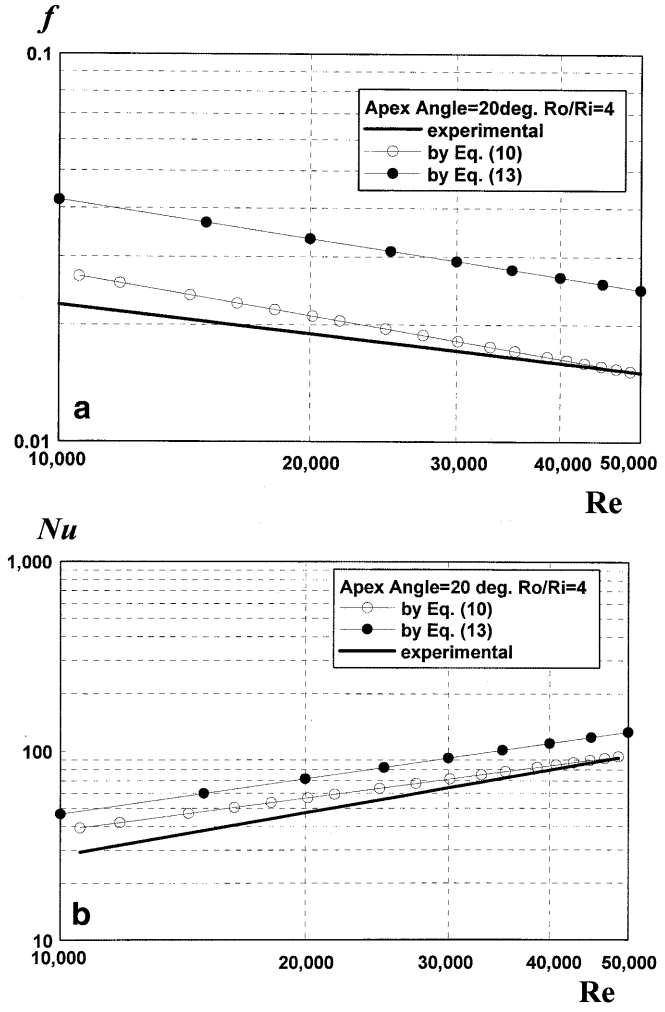

Fig. 2. Effect of the definitions of u^+ and y^+ on the numerical results. (**a**) Effect on friction factor, (**b**) Effect on Nusselt number

where S_{ij} and D_{ij} are terms related to the curvature if cylindrical coordinate is used [15, 16]. There are many different methods to modelize the above equation. In the FLUENT the method by Launder [15] is used to modelize the diffusion term, pressure-strain term and viscos dissipation term. The boundary conditions are given explicitly.

3
Numerical methods

The discretized forms of the governing equations were derived by integrating the equations over a finite control volume. The resulted algebraic equations were of diffusion-type and solved by SLUR method in conjunction with TDMA.

When the k–ε model with wall function is used, the following condition should be satisfied while choosing the first internal points in the vicinity of the wall.

$$11.5 \leq x_p^+, y_p^+ \leq 400 \qquad (15)$$

where x_p^+, y_p^+ are the dimensionless circumferential and radial coordinates, respectively, of the first internal points. The "large coefficient method" proposed in [17] was used for assigning the specified values of turbulent dissipation from Eq. (11) to the first internal points in the vicinity of the wall.

In using the FLUENT software, the calculation of the fully developed flow and heat transfer is realized by defining the inlet and outlet boundary conditions of a three dimensional solution domain as the periodic fully developed ones.

4
Results and discussion

Computations were first performed to find out the most suitable value of a_1 in the mixing length theory, the ratio of R_m/R_i and the appropriate range of x_p^+, y_p^+ in the two-equation turbulence model for the cases studied. In the presentation followed, some results related to the preliminary computations will be first presented, followed by the friction factor and heat transfer results of the three turbulence models in the test parameter range of Ref. [10]. Then the results of extended computations for heat transfer are provided.

The major findings in our preliminary computations are as follows. For the mixing length theory the most suitable value of the adjustable coefficient a_1 is 0.7, and this value is used for all the computations when this model was adopted. It is also found that the iteration could converge more rapidly if a non-uniform grid distribution was used, with more grid points clustered near the surface. The results of the ratio of R_m/R_i are listed in Tables 3 and 4. It can be seen that this ratio is dependent on the ratio of

Table 3. Comparison of predicted and iteratively computed value of R_m/R_i ($\theta_0 = 40°$)

R_o/R_i	Re	R_m/R_i	
		Predicted by Eq. (8)	Iteratively determined
2	10,000 100,000	1.4408	1.5467
3	10,000 100,000	1.8138	2.2068
4	10,000 100,000	2.1499	2.7524
5	10,000 100,000	2.4616	3.2669

Table 4. Comparison of predicted and iteratively computed value of R_m/R_i ($R_o/R_i = 4$)

θ_0	R_m/R_i	
	Predicted by Eq. (8)	Iteratively determined
40	2.1499	2.7524
30	2.1499	2.9161
24	2.1499	3.0157
20	2.1499	3.1105
18	2.1499	3.1561

R_o/R_i and the apex angel. Generally, the numerical computed values are larger than what are predicted by the equation for a concentric annulus. The larger the radius ratio and the smaller the apex angle, the higher the deviation. The deviation ranges from 7% for $\theta_0 = 40^\circ$ and R_o/R_i = 2–65% for $\theta_0 = 18^\circ$ and $R_o/R_i = 5$. For the standard k–ε model it was found that the numerical heat transfer results obtained with $20 \leq x_p^+, y_p^+ \leq 30$ agreed with the test data most satisfactorily.

In order to obtain the grid-independent solutions using mixing length theory, the numerical calculations are conducted on the four grids with different grid numbers for the following case: $R_o/R_i = 4$, Re = 35000 and $\theta_0 = 40^\circ$. Some numerical results and the results from Richardson extrapolation [18] are listed in Table 5. Considering the balance between accuracy and economics, the first grid system is chosen for all the computations, and the estimated relative errors are 2.77 and 2.36% for the computed friction factors and Nusselt numbers, respectively.

For the k–ε model with wall function, it is more important to satisfy the condition (15) than to refine the grid. So the grid number 42 × 52 is chosen, which can keep x_p^+, y_p^+ in the range from 20 to 30 during the numerical computations.

In the following section, the results are first presented for the cases tested in [10], followed by the results of extended computations in which both the ratio of R_o/R_i and the Reynolds number range are extended.

Fluid flow characteristics

The friction factor is defined as

$$f = -\frac{dp}{dz} D_e/(0.5 \cdot \rho w_b^2) \qquad (16)$$

where D_e and w_b are hydraulic diameter and mean velocity at the cross-section, respectively.

Using the three turbulent models mentioned above, the predicted variations of the friction factor in the fully developed region with the Reynolds number are shown in Figs. 3–5, respectively. Figure 6 is the experimental results by Tao et al. [10]. Clearly, none of the predicted results from the three turbulence models are satisfactory. The major disagreements are as follows. The experimental results show that at the same Reynolds number the friction factor decreases with the decrease in apex angle. This variation trend is seemingly consistent with some existed test results for other non-circular geometry [19]. The predicted results from mixing length theory and k–ε model show some insensitivity of the friction factor to the apex angle, only the results of the Reynolds stress model exhibit the same trend with an appreciably quantitative difference. As far as the slope in f–Re curve is concerned, the results from mixing length theory and Reynolds stress model are quite agreeable with the test data. More research work is needed to achieve satisfactory numerical results for friction factors both qualitatively and quantitatively.

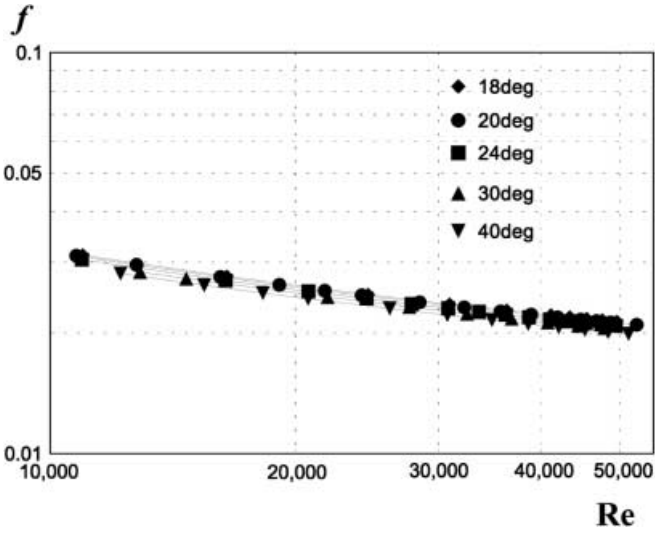

Fig. 3. Variation of friction factor with the Reynolds number (the mixing length theory)

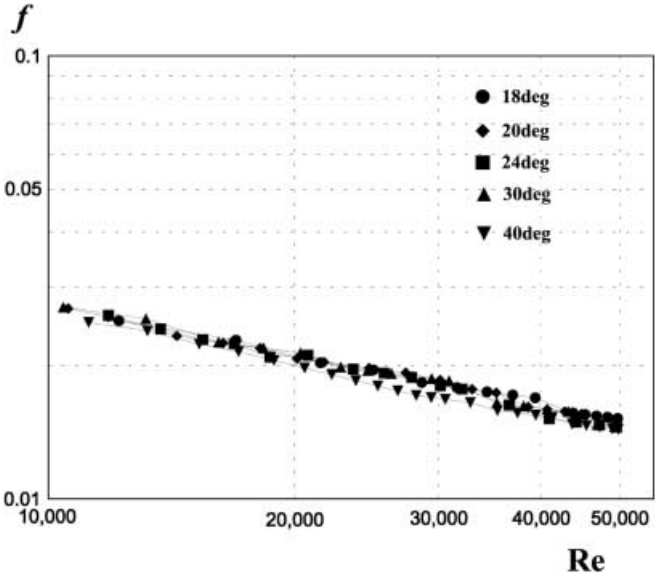

Fig. 4. Variation of friction factor with the Reynolds number (k–ε model)

Table 5. Grid – independent examination

	The mixing length theory Grid points				Richardson extrapolation
	42 × 52	66 × 66	82 × 82	102 × 102	
$f(\times 10^{-2})$	2.1639	2.1440	2.1212	2.1163	2.1055
Nu	71.216	70.908	70.116	69.793	69.571

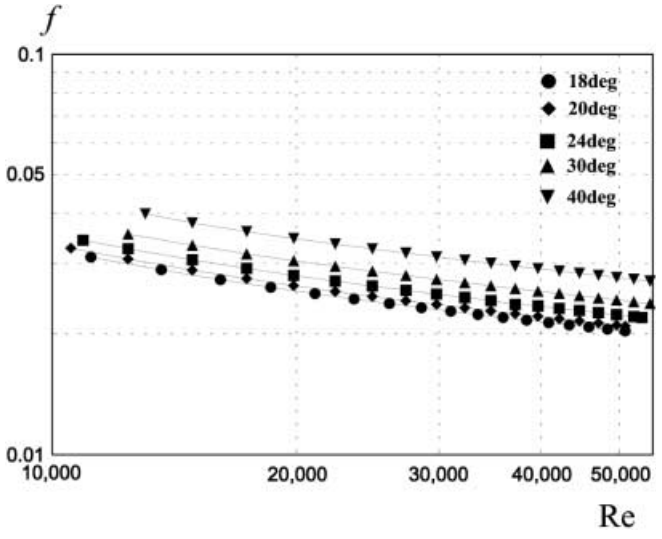

Fig. 5. Variation of friction factor with the Reynolds number (the Reynolds stress model)

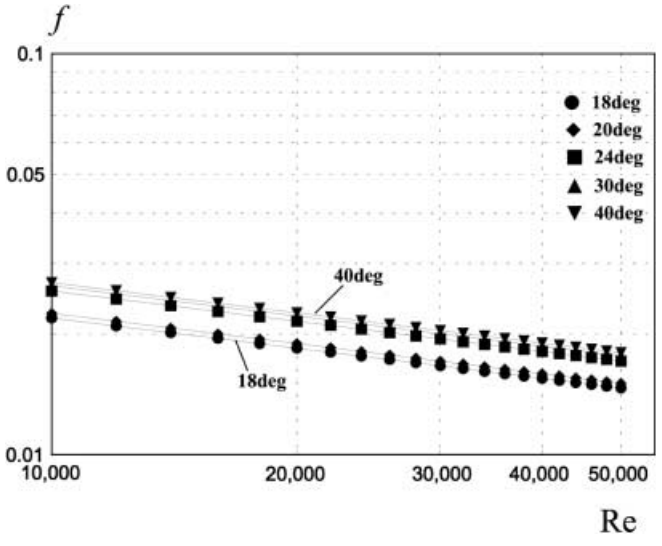

Fig. 6. Variation of friction factor with the Reynolds number (the experimental results)

Heat transfer characteristics

It is well known that in the fully developed region the effect of the thermal boundary condition on the heat transfer can be neglected [20]. In order to accelerate the iterative convergence, the first kind of boundary condition was applied to the annular surface. That is the outer surface of the annular-sector configuration was assumed to be at constant temperature. Computations were conducted for air with Pr = 0.703.

The bulk temperature of the fluid is defined as

$$T_{\mathrm{b}} = \iint \rho w T r \,\mathrm{d}r\,\mathrm{d}\theta \Big/ \iint \rho w r \,\mathrm{d}r\,\mathrm{d}\theta \tag{17}$$

According to the heat balance, the mean heat transfer coefficient can be derived as

$$\alpha = \frac{\rho w_b A c_p \mathrm{d}T_{\mathrm{b}}/\mathrm{d}z}{S(T_{\mathrm{w}} - T_{\mathrm{b}})} \tag{18}$$

where S and A are the heat transfer area and the cross-section area, respectively. The Nusselt number is defined as

$$\mathrm{Nu} = \alpha D_e / k \tag{19}$$

The variations of the Nusselt number with the Reynolds number are shown in Figs. 7–9 for the three turbulence models, respectively. The experimental results in [10] can be well-correlated by the following equation

$$\mathrm{Nu} = 0.0281\mathrm{Re}^{0.75} \tag{20}$$

This equation is shown by a solid line in the above three figures for comparison. It is found that very satisfactory results are obtained using the mixing length theory ($a_1 = 0.7$). While as a whole the k–ε model with wall function over-predicts the heat transfer rate, with increasing deviation when the Reynolds number decreases. The predicted results from the Reynolds stress exhibit

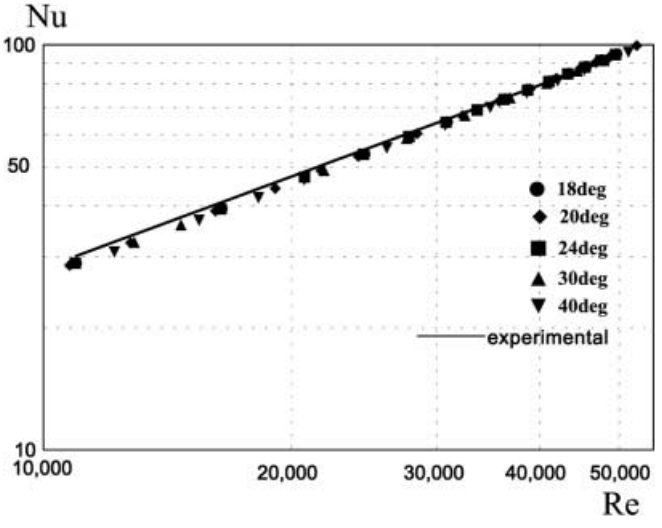

Fig. 7. Variation of the Nusselt number with the Reynolds number (the mixing length theory)

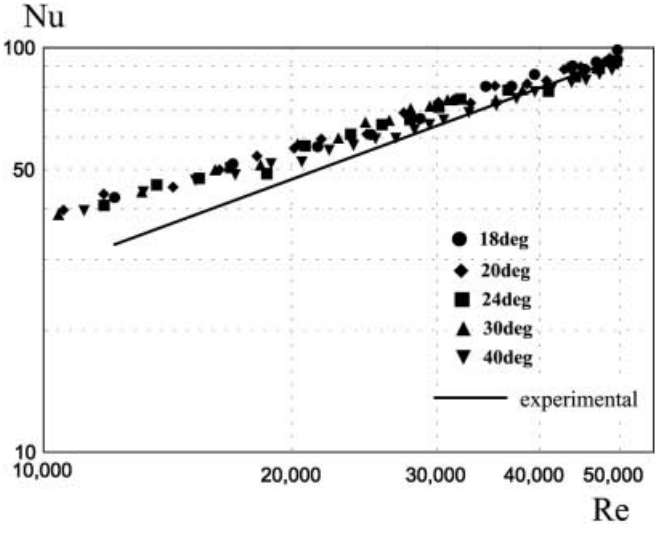

Fig. 8. Variation of the Nusselt number with the Reynolds number (the k–ε model)

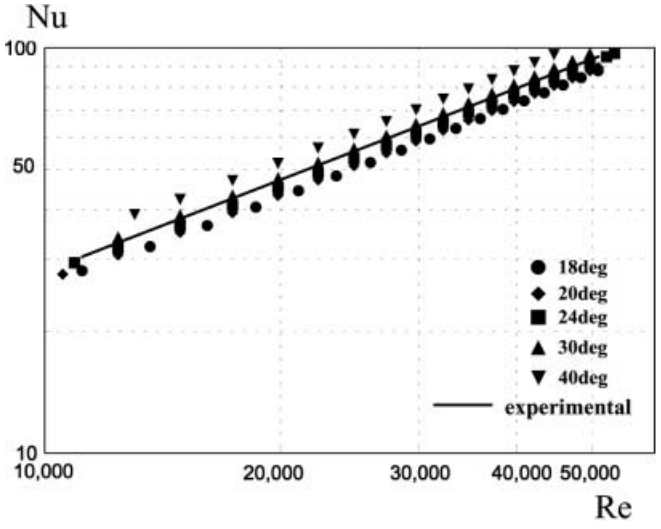

Fig. 9. Variation of the Nusselt number with the Reynolds number (the Reynolds stress model)

systematic and appreciable apex angle sensitivity, with the largest apex angle having the highest Nusselt number. At the same Reynolds number the Nusselt number of the duct with an apex angle of 40°is about 23% higher than the Nusselt number of 18°. Such appreciably and systematic sensitivity was not observed in the test data of [10].

The secondary flow contribution at the cross-section
Previous numerical simulation [21, 22] of fully developed turbulent fluid flow in non-circular tubes indicated that there are secondary flows at the cross-section although the flow is fully developed. In our numerical simulation, such a secondary flow can not be captured by using the mixing length theory and the k–ε model, since the governing equations therein contain only the axial velocity w and the temperature T. Numerical simulations are conducted for revealing this secondary flow by using the Reynolds stress model. The velocity vectors at the cross section as shown in Fig. 10 for three apex angles. Clearly, the secondary flow mainly lies in the four corners. Moreover, the strength of the secondary flow weakens with the increase in apex angle. Maybe this is one of the reasons that the numerical results of the friction factors using the mixing length theory and the k–ε model do not show appreciable apex angle sensitivity. However, our numerical practices show that the secondary flow does not have strong effect on the average heat transfer behavior in the fully developed region.

Results of the other cases of different ratios of R_o/R_i
According to the above comparisons of the numerical results with those of the experiments, from the considerations of both agreement and computational time and memory, the mixing length theory is considered the best among the three models to predict the fully developed heat transfer behavior for the annular sector ducts. Therefore further investigations are performed to extend the ranges of the radius ratio, R_o/R_i, and the Reynolds number. Computations are conducted for the five apex angles with radius ratio of 2, 3, and 5, and within the Reynolds number range from 10^4 to 10^5. The heat transfer results for apex angles of 18 and 40° are shown in Figs. 11, 12. In the figures the results for $R_o/R_i = 4$ and Eq. (20) are also presented for comparison. It can be seen that numerical results agree very well with the experimental correlation within the parameter range studied, with a maximum deviation less than 8.3%. Similar results are also obtained for

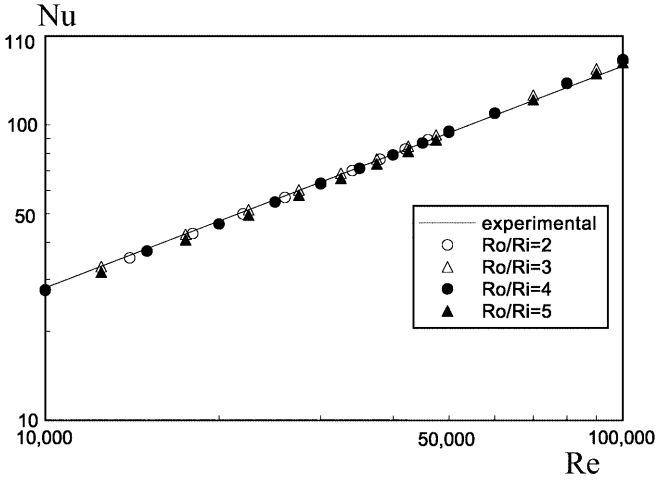

Fig. 11. Heat transfer characteristics ($\theta = 18°$)

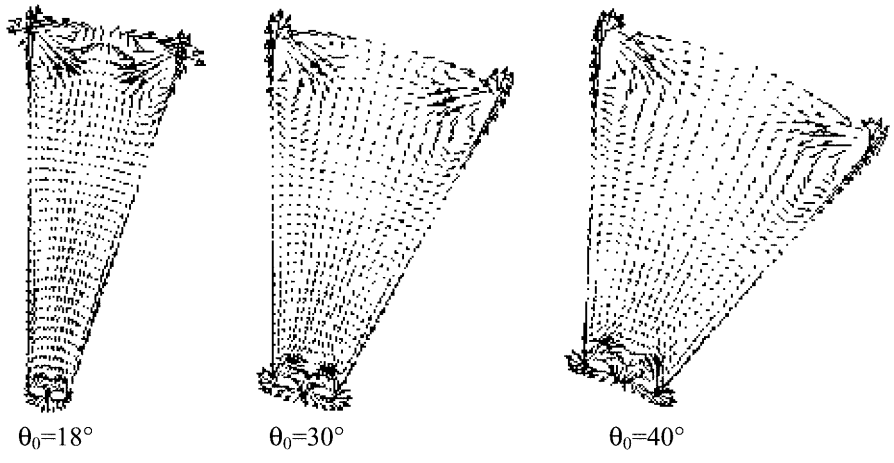

Fig. 10. Contributions of the secondary flow at the cross section with different apex angle

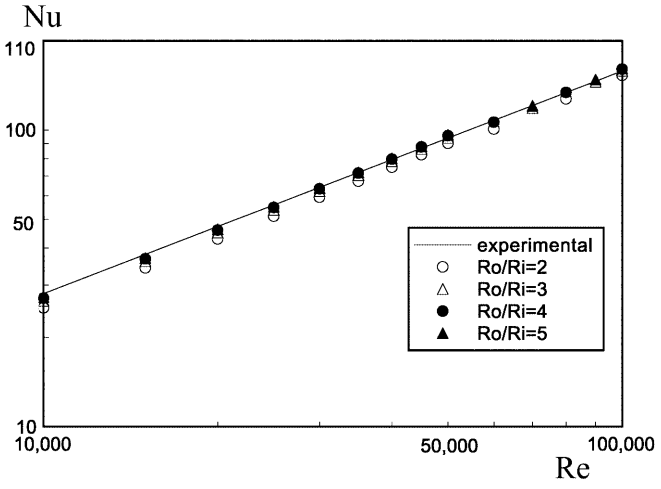

Fig. 12. Heat transfer characteristics ($\theta = 18°$)

the other three apex angles, and for simplicity they are not reproduced here.

Finally, the axial velocity and temperature contours for the case of $\theta_0 = 40°, R_o/R_i = 4$ and Re = 35000 are presented in Fig. 13. It can be seen that the contour shapes of the non-dimensional axial velocity and non-dimensional temperature in the fully developed region resemble each other, in which lies the basis of the approximate theory of the Reynolds analogy. It may be interesting to show the intermediate results of the velocity and temperature contours when Eq. (8) is used to specify the ratio of R_m/R_i. These are shown in Fig. 14. Apart from the shape difference in contour lines, careful inspection of Fig. 14a reveals that the intermediate results of axial velocity contours actually gives a larger value of R_m/R_i than it is predicted by Eq. (8) (2.1499 for this case). Therefore iteration must be conducted to eliminate the inconsistency between the specified and computed value of R_m/R_i.

5 Conclusion

Using the mixing length theory, k–ε model and Reynolds stress model, numerical study has been conducted for the fully developed turbulent fluid flow and heat transfer in annular-sector ducts having apex angles ranged from 18 to 40°. Comparisons of numerical results with available test data are conducted. Following conclusions may be drawn:

1. None of the three turbulence models can predict the fully developed friction factors which agree well with the test data both qualitatively and quantitatively. In the results of the Reynolds stress model, the variation trend of the friction factor with the apex angle agree with the experiments with an appreciably over-prediction deviation. The Reynolds stress model can resolute the cross section secondary flow. And it is found that the secondary flow mainly lies in the four corners and the strength of the secondary flow weakens with the increase in apex angle. Further research is needed to improve the model for more accurate prediction of the flow characters.

2. For simulation of the fully developed heat transfer character, the mixing length theory seems the best for the

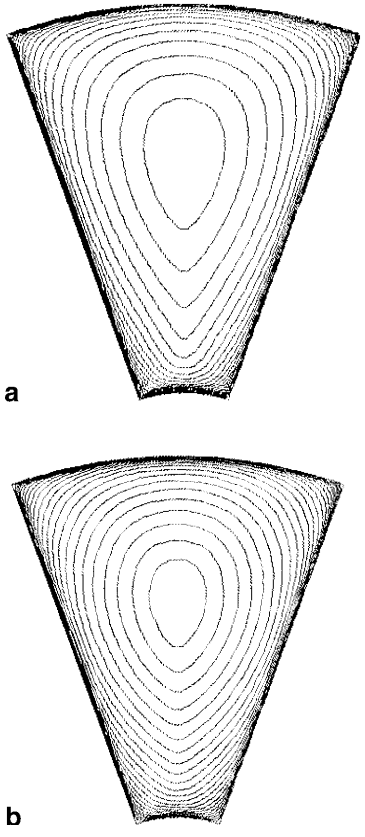

Fig. 13a,b. Contours of dimensionless velocity and temperature (R_m/R_i determined iteratively)

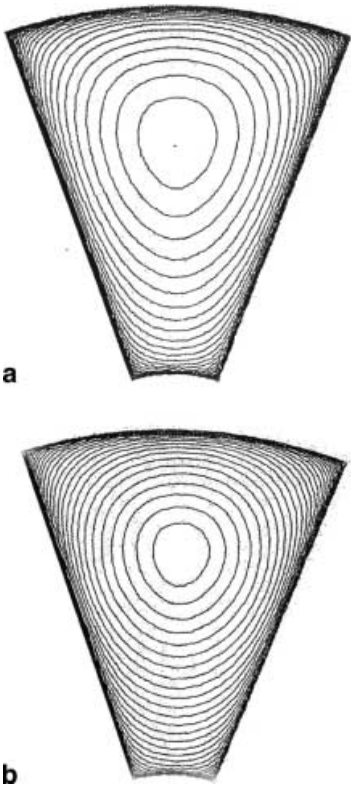

Fig. 14a,b. Contours of dimensionless velocity and temperature (R_m/R_i determined by Eq. (8))

cases studied. With iteratively determined ratio of R_m/R_i, the mixing length theory is adopted to predict heat transfer for the following parameter range: $\theta_0 = 18, 20, 24, 30$ and 40°, $R_o/R_i = 2, 3, 4, 5$ and $Re = 10^4$–10^5. Numerical results agree with the available correlation very satisfactorily with the maximum deviation of 8.3%. Thus present numerical work demonstrates that the application range of Eq. (20) can be extended to the parameter range indicated above, though its original test range is $\theta_0 = 18, 20, 24, 30$ and 40°, $R_o/R_i = 4$, and $Re = 10^4$–5×10^5.

References

1. **Sparrow EM; Chen TS; Johnson VK** (1964) Laminar flow and pressure drop in internally finned annular ducts. Int J Heat Mass Transfer 7: 583–585
2. **Webb RL** (1994) Principles of Enhanced Heat Transfer. John Wiley & Sons, Inc., New York
3. **Taborek J** (1997) Double-pipe and multi-tube heat exchangers with plain and longitudinal finned tubes. Heat Transfer Eng 18: 34–45
4. **Ebadian MA; Dong ZF** (1998) Forced convection, internal flow ducts. In: Rohsenow WM; Hartnett JP; Cho YI, (eds.). Handbook of Heat Transfer, 3rd edn., McGraw Hill, New York
5. **Soliman HM; Mennis AA; Trupp AC** (1982) Laminar flow in entrance region of circular sector duct. J Appl Mech 49: 640–642
6. **Soliman HM** (1987) Laminar heat transfer in annular sector ducts. ASME J Heat Transfer 109: 247–249
7. **Ben-Ali TM; Soliman HM; Zariffeh EK** (1989) Further results for laminar heat transfer in annular section and circular sector ducts. ASME J Heat Transfer 111: 1090–1093
8. **Lin MJ; Wang QW; Tao WQ** (2000) Developing laminar flow and heat transfer in annular-sector ducts. Heat Transfer Eng 21(2): 53–61
9. **Carnavos TC** (1978) Cooling air in turbulent flow with multipassage internally finned tubes, ASME paper 78-WA/HT-52
10. **Tao WQ; Lu SS; Kang HJ; Lin MJ** (2000) Experimental study on developing and fully developed fluid flow and heat transfer in annular-sector ducts. J Enhanced Heat Transfer 7: 51–60
11. **Tao WQ** (1988) Numerical Heat Transfer. Xi'an Jiaotong University Press, Xi'an, China
12. **Patankar SV; Ivanovic M; Sparrow EM** (1979) Analysis of turbulent flow and heat transfer in internally finned tubes and annuli. ASME J Heat Transfer 101: 29–37
13. **Yueh Yuh-Shan; Chieng Ching-Chang** (1987) On the calculation of flow and heat transfer characteristics for CANDU-type 19-rod fuel bundles. ASME J Heat Transfer 109: 590–598
14. **Launder BE; Spalding DB** (1974) The numerical computation of turbulent flows. Comp Meth Appl Mech Eng 3: 269–289
15. **Launder BE; Reece GJ; Rodi W** (1975) Progress in the development of a Reynolds-stress turbulence closure. J Fluid Mech 68: 537–566
16. **Launder BE** (1989) Second-moment closure: present... and future?, Int J Heat Fluid Flow 10(4): 282–300
17. **Yang M; Tao WQ** (1992) Numerical study of natural convection heat transfer in a cylindrical envelope with internal concentric slotted hollow cylinder. Numer Heat Transfer, Part A 22: 289–305
18. **Roache PJ** (1994) Prospective: a method for uniform reporting of grid refinement studies. ASME J Fluid Eng 116: 405–413
19. **Rehsenow WH; Hartnett JP; Ganic EN** (1985) Handbook of Heat Transfer Fundamentals. 2nd edn., McGraw Hill, New York, pp. 7.98–7.100
20. **Kays WM; Crawford MF** (1980) Convective Heat Transfer and Mass Transfer, 2nd edn. McGraw Hill, New York
21. **Nakayama A; Chow WL; Shama D** (1983) Calculation of fully developed turbulent flows in ducts of arbitrary cross-section. J Fluid Mech 128: 199–217
22. **Yang G; Ebadian MA** (1991) Effect of Reynolds number and Prandtl numbers on turbulent heat transfer in a three-dimensional square duct. Numer Heat Transfer, Part A 20: 111–122